

Chirality Dependent Intrinsic Thermal Conductivity in Single-Layer MoS₂

Jin-Wu Jiang* and Timon Rabczuk†

*Institute of Structural Mechanics, Bauhaus-University Weimar,
Marienstr. 15, D-99423 Weimar, Germany*

(Dated: March 25, 2013)

Abstract

We investigate the thermal conductivity in the armchair and zigzag MoS₂ nanoribbons, by combining the non-equilibrium Green's function approach and the first-principles method. A strong chirality dependence is observed in the thermal conductivity. Particularly, the thermal conductivity for the armchair MoS₂ nanoribbon is about 25% lower than that in the zigzag nanoribbon at room temperature. By calculating the Caroli transmission, we disclose the underlying mechanism for this strong chirality dependence to be the much less phonon transport channels in the armchair MoS₂ nanoribbon in the frequency range of [150, 300] cm⁻¹.

PACS numbers: 65.80.Ck, 63.22.Np, 68.65.-k

Keywords: thermal conductivity, single-layer MoS₂, chirality dependence, anisotropy

The two-dimensional single-layer MoS₂ (SLMS) has drawn considerable interest in recent years, owing to its direct band gap and graphene-like layered honeycomb lattice structure.^{1–18} The band gap in the SLMS is a great advantage over graphene, which has zero band gap without the help of strain or other gap-opening techniques. Thus, the SLMS becomes a promising alternative to graphene in many electronic fields. For this purpose, many efforts have been devoted to comparatively investigate various properties of the SLMS and the graphene. It was found that the interface between the SLMS and the gold metal is inefficient for electron injection; while the Ti metal can greatly improve the efficiency.⁵ The mechanical and electronic properties of the SLMS have been investigated by first-principles calculations, where the defects were found to play an important role.⁶ Sánchez and Wirtz studied the phonon properties of the SLMS, using the first-principles calculations.⁷

In a very recent experiment, Sahoo *et.al* measured the thermal conductivity in the SLMS through analyzing the laser power dependence of the Raman mode.⁸ The obtained thermal conductivity is 52 Wm⁻¹K⁻¹ at room temperature. The thermal conductivity is an important parameter for possible applications of the SLMS. High thermal conductivity is helpful to deliver heat away from the electronic device, which is good to prevent heating induced breakdown of the device. For thermoelectric applications, lower thermal conductivity can yield in higher figure of merit ZT.^{19–21} Hence, it is useful to provide an accurate prediction for the intrinsic thermal conductivity value, i.e the thermal conductivity in a pure SLMS without any phonon decaying mechanism. This intrinsic thermal conductivity can serve as an upper limit for the values from the experimental measurement or other theoretical calculations.

In this letter, we comparatively study the thermal conductivity in both armchair and zigzag MoS₂ nanoribbons (MSNRs), by using the ballistic non-equilibrium Green's function (NEGF) formalism and the first-principles calculations. We find that the thermal conductivity is strongly dependent on the chirality. The room temperature thermal conductivity in the armchair MSNR is about 25% lower than that of the zigzag MSNR. The Caroli transmission function shows that the origin for the strong chirality dependence is because of the much less phonon transport channels in the armchair MSNR in the frequency range of [150, 300] cm⁻¹.

In the *ab initio* calculation, we use the SIESTA package²² to optimize the structure of the SLMS. The local density approximation is applied to account for the exchange-correlation

function with Ceperley-Alder parametrization²³ and the double- ζ basis set orbital is adopted. During the conjugate-gradient optimization, the maximum force on each atom is smaller than $0.01 \text{ eV}\text{\AA}^{-1}$. A mesh cut off of 120 Ry is used. Periodic boundary condition is applied in the heat current direction and the in-plane transverse direction. The free boundary condition is applied to the out-of-plane direction by introducing sufficient vacuum space. There are two types of calculations in this work. In the calculation of the phonon spectrum, a small unit cell is used and an $8 \times 1 \times 1$ Monkhorst-Pack k -grid is chosen for the sampling of the quasi-one-dimensional Brillouin zone. In the investigation of the thermal transport, a large unit cell is calculated and the Gamma point k sampling is adopted.

The relaxed structures for armchair and zigzag MSNRs are shown in Fig. 1. The Mo-S bond length is 2.414 \AA , which is between the value 2.382 \AA from Sánchez *et.al*⁷ and 2.42 \AA from Ataca *et.al*.⁶ There are 36 (18) atoms in the smallest translation unit cell in the armchair (zigzag) MSNR. Fig. 2 compares the phonon dispersion in the armchair (left) and zigzag (middle) MSNRs. Two smallest translation unit cells are included for the armchair MSNR in the calculation of the phonon dispersion. For the zigzag MSNR, four smallest translation unit cells have been used. Hence there are 72 atoms involved in the calculation, resulting in 216 phonon branches in both panels. The wave vector k is along the heat current direction and in the unit of $2\pi/a$, with $a = 10.705 \text{ \AA}$ or 12.364 \AA in the armchair or zigzag MSNR, respectively. An obvious band gap around 300 cm^{-1} is found in the phonon spectra for both armchair and zigzag MSNRs. Similar band gap has been found in some existing works.^{6,7} The three acoustic phonon branches from the armchair and zigzag MSNRs are compared in the right panel. We note that the x axis here is in the unit of \AA^{-1} , which is different from the left and middle panels in the same figure. It is obvious that the armchair MSNR has considerably higher phonon spectrum than the zigzag MSNR. It should be noted that the out-of-plane transverse branch should behave flexibly due to the two-dimensional nature of the SLMS. This flexure nature disappears in present calculation, due to the loss of the rigid rotational invariance symmetry in the *ab initio* calculation.²⁴

There are various options to investigate the thermal transport. Classical results can be obtained from the molecular dynamics simulation of the thermal transport, where the phonon-phonon scattering dominates the transport process. From the theoretical point of view, it is a big challenge to provide accurate prediction for the thermal conductivity, because the samples in the experiment always possess various unpreventable defects. Hence,

a more practical task is to provide an accurate (quantum) prediction for the upper limit of the thermal conductivity. For this purpose, we would rather apply the ballistic NEGF method.^{25,26} It is based on quantum mechanics. The phonon-phonon scattering is ignored in the ballistic transport region, which is actually quite reasonable for low-dimensional nanomaterials. For instance, in graphene, it has been found that the out-of-plane transverse phonon mode can transport almost ballistically even in a large piece of graphene.²⁷ The combination of the NEGF and the *ab initio* calculation can provide us an accurate upper limit for the thermal conductivity.²⁸

In the NEGF approach, the thermal conductance is calculated by the Landauer formula:

$$\sigma = \frac{1}{2\pi} \int d\omega \hbar \omega T[\omega] \left[\frac{\partial n(\omega, T)}{\partial T} \right], \quad (1)$$

where \hbar is the Planck's constant. $n(\omega, T)$ is the Bose-Einstein distribution function. The transmission $T[\omega]$ is obtained from the Caroli formula:

$$T[\omega] = \text{Tr} (G^r \Gamma_L G^a \Gamma_R), \quad (2)$$

where G^r is the retarded Green's function. $G^a = (G^r)^\dagger$ is the advanced Green's function and $\Gamma_{L/R}$ is the self-energy. These Green's functions can be calculated from the force constant matrix from the *ab initio* calculation.²⁸

Fig. 3 top panel shows the transmission functions for the armchair and zigzag MSNRs. These functions exhibit some regular steps, due to the absence of phonon-phonon scattering. In the ballistic transport, σ is proportional to the cross-sectional area, since there are more channels available for heat delivery in thicker nanoribbons. However, the thermal conductance from Eq. 1 does not depend on the length of the system. σ can be used to get the thermal conductivity (κ) of a MSNR with arbitrary length L : $\kappa = \sigma L/s$, where s is the cross-sectional area. We have assumed the thickness of the MSNR to be 6.033 Å, which is the space between two adjacent layers in the bulk MoS₂.⁷ This thickness value is the same for both armchair and zigzag MSNRs, so its value does not affect our comparison for their thermal conductivity. It is quite obvious that the thermal conductivity does not depend on the cross section. It means that the thermal conductivity in the MSNR does not depend on its width, since the thickness is a constant. On the other hand, the thermal conductivity in ballistic region increases linearly with increasing length, which has been observed in the thermal conductivity of two-dimensional graphene.^{27,29–32} In the experiment, the thermal

conductivity is measured for a MSNR sample of dimension around μm .⁸ Hence, we will predict the thermal conductivity for a MSNR of length $L = 1.0 \mu\text{m}$.

Fig. 3 bottom panel gives the thermal conductivity for both armchair and zigzag MSNRs of $1.0 \mu\text{m}$ in length. A strong chirality dependence is revealed in the thermal conductivity. The thermal conductivity in the armchair MSNR is smaller than that of the zigzag MSNR in the whole temperature range. The chirality-induced anisotropy is about 25% at room temperature. This anisotropy is much stronger than that in the graphene. In the ballistic region, the chirality-induced anisotropy is only about 1% in the single-layer graphene.³²

The top panel in the figure discloses the origin for this strong anisotropy. It is because the transmission function in the armchair MSNR is much smaller than that of the zigzag MSNR in the frequency range $[150, 300] \text{ cm}^{-1}$. It means that the phonon transport channels are much less in this frequency domain for armchair MSNR, leading to much smaller thermal conductivity in the armchair MSNR, although the three acoustic velocities in the armchair MSNR are higher as shown in Fig. 2 right panel. Particularly, the room-temperature thermal conductivity is 673.6 and $841.1 \text{ Wm}^{-1}\text{K}^{-1}$ in armchair and zigzag MSNRs. These values are about one third of the superior thermal conductivity value (around $3000 \text{ Wm}^{-1}\text{K}^{-1}$) in the graphene,²⁹ because the overall phonon spectrum in the MSNR ($[0, 500] \text{ cm}^{-1}$) is scaled by a factor of one third from the phonon spectrum in the graphene ($[0, 1600] \text{ cm}^{-1}$). The experiment value is $52 \text{ Wm}^{-1}\text{K}^{-1}$, which is far below our quantum upper limit. It indicates strong phonon scattering or substrate-induced phonon leaking effects in the experimental samples, as suggested by the authors in Ref. 8.

We should stress that our theoretical value serves as an upper limit for the thermal conductivity of the $1.0 \mu\text{m}$ MSNRs. If the experimental samples are of high quality, then the measured thermal conductivity should approach 673.6 or $841.1 \text{ Wm}^{-1}\text{K}^{-1}$ from lower side.

In conclusion, we have applied the ballistic NEGF approach to predict the upper thermal conductivity value in the armchair and zigzag MSNRs. The force constant matrix is calculated from the first-principles method. A strong chirality dependence is found in the thermal conductivity. More specially, the thermal conductivity in the armchair MSNR is about 25% smaller than the zigzag MSNR at room temperature. The Caroli transmission function discloses the origin for this strong anisotropy to be the much less transport channels in the armchair MSNR in the frequency range of $[150, 300] \text{ cm}^{-1}$.

Acknowledgements The work is supported by the Grant Research Foundation (DFG).

- * Electronic address: jwjiang5918@hotmail.com
- [†] Electronic address: timon.rabczuk@uni-weimar.de
- ¹ P. Joensen, E. D. Crozier, N. Alberding, and R. F. Frindt, *Journal of Physics C: Solid State Physics* **20**, 4043 (1987).
- ² S. Helveg et al., *Physical Review Letters* **84**, 951 (2000).
- ³ K. F. Mak, C. Lee, J. Hone, J. Shan, and T. F. Heinz, *Physical Review Letters* **105**, 136805 (2010).
- ⁴ C. Lee et al., *ACS Nano* **4**, 26952700 (2010).
- ⁵ I. Popov, G. Seifert, and D. Tománek, *Physical Review Letters* **108**, 156802 (2012).
- ⁶ C. Ataca, H. Sahin, E. Aktürk, and S. Ciraci, *Journal of Physical Chemistry C* **115**, 39343941 (2011).
- ⁷ A. Molina-Sánchez and L. Wirtz, *Physical Review B* **84**, 155413 (2011).
- ⁸ S. Sahoo, A. P. S. Gaur, M. Ahmadi, M. J.-F. Guinel, and R. S. Katiyar, *Arxiv.org* (2013).
- ⁹ Z. Yin et al., *ACS Nano* **6**, 74 (2011).
- ¹⁰ K. Chang and W. Chen, *Journal of Materials Chemistry* **21**, 17175 (2011).
- ¹¹ C. Ataca and S. Ciraci, *Journal of Physical Chemistry C* **115**, 13303 (2011).
- ¹² A. Castellanos-Gomez et al., *Nano Letters* **12**, 31873192 (2012).
- ¹³ J. N. Coleman et al., *Science* **331**, 568 (2011).
- ¹⁴ K.-K. Liu et al., *Nano Letters* **12**, 1538 (2012).
- ¹⁵ D. Le, D. Sun, W. Lu, L. Bartels, and T. S. Rahman, *Physical Review B* **85**, 075429 (2012).
- ¹⁶ J. Brivio, D. T. L. Alexander, and A. Kis, *Nano Letters* **11**, 51485153 (2011).
- ¹⁷ B. Radisavljevic, A. Radenovic, J. Brivio, V. Giacometti, and A. Kis, *Nature Nanotechnology* **6**, 147 (2011).
- ¹⁸ B. Radisavljevic, M. B. Whitwick, and A. Kis, *Applied Physics Letters* **101**, 043103 (2012).
- ¹⁹ H. J. Goldsmid, *Thermoelectric Refrigeration*, Plenum, New York, 1964.
- ²⁰ H. J. Goldsmid, *Electronic Refrigeration*, Pion, London, 1986.
- ²¹ G. S. Nolas, J. Sharp, and J. Goldsmid, *Thermoelectrics: Basic Principles and New Materials Developments*, Springer, New York, 2001.

- ²² J. M. Soler et al., Journal of Physics: Condensed Matter **14**, 2745 (2002).
- ²³ D. M. Ceperley and B. J. Alder, Physical Review Letters **45**, 566 (1980).
- ²⁴ J.-W. Jiang, H. Tang, B.-S. Wang, and Z.-B. Su, Physical Review B **73**, 235434 (2006).
- ²⁵ J.-S. Wang, J. Wang, and J. T. Lü, Eur. Phys. J. B **62**, 381 (2008).
- ²⁶ J.-W. Jiang, J.-S. Wang, and B. Li, Journal of Applied Physics **109**, 014326 (2011).
- ²⁷ D. L. Nika, E. P. Pokatilov, A. S. Askerov, and A. A. Balandin, Physical Review B **79**, 155413 (2009).
- ²⁸ J.-W. Jiang, B.-S. Wang, and J.-S. Wang, Applied Physics Letters **98**, 113114 (2011).
- ²⁹ A. A. Balandin et al., Nano Letters **8**, 902 (2008).
- ³⁰ D. L. Nika, S. Ghosh, E. P. Pokatilov, and A. A. Balandin, Applied Physics Letters **94**, 203103 (2009).
- ³¹ A. A. Balandin, Nature Materials **10**, 569 (2011).
- ³² J.-W. Jiang, J.-S. Wang, and B. Li, Physical Review B **79**, 205418 (2009).

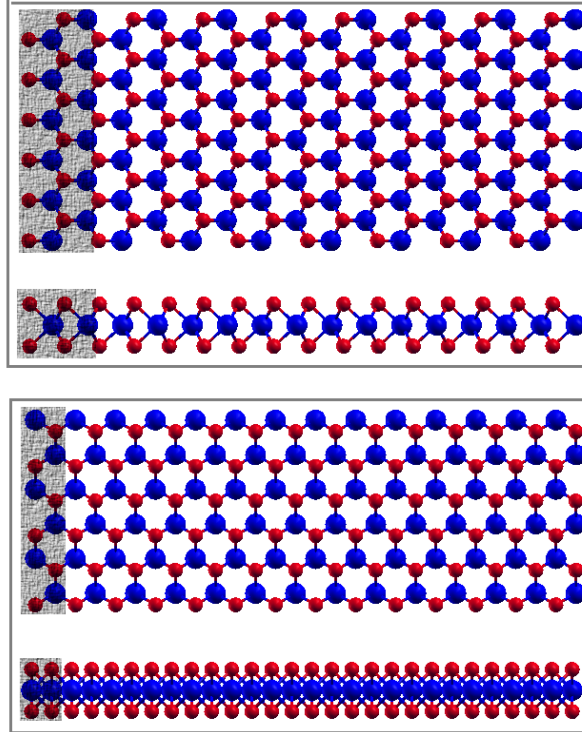


FIG. 1: (Color online) The relaxed structure of the armchair (top) and zigzag (bottom) MSNRs. Top and side views are shown for each system. Atoms are denoted by blue (Mo) and red (S). The translation unit cells are highlighted on the left end.

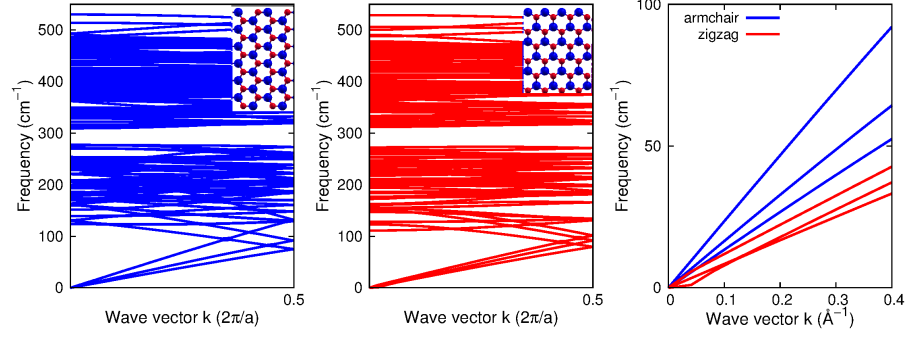


FIG. 2: (Color online) Phonon dispersion in armchair (left) and zigzag (middle) MSNRs. Insets show the unit cells used in the calculation of the phonon spectrum. The three acoustic phonon branches in armchair and zigzag systems are compared in the right panel. We note the band gap around 300 cm^{-1} in the spectrum.

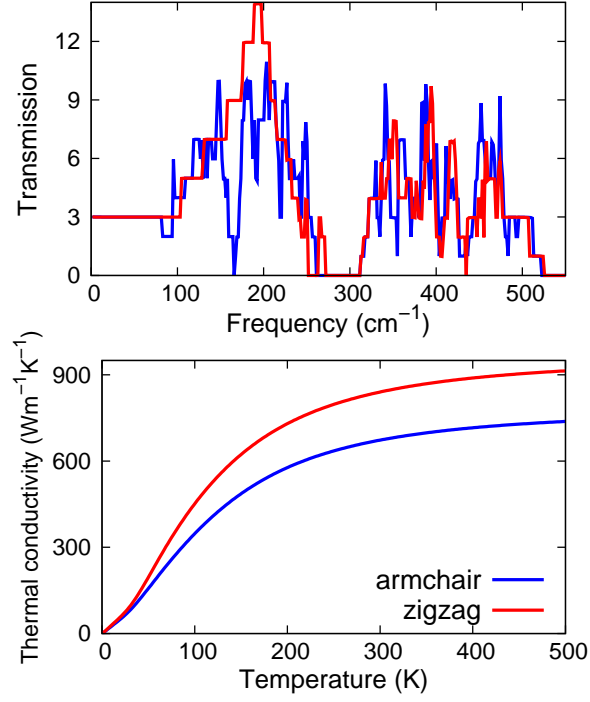


FIG. 3: (Color online) Top: the transmission functions for armchair and zigzag MSNRs. Note obvious less transmission channels in the armchair MSNR in $[150, 300] \text{ cm}^{-1}$. Bottom: the thermal conductivity (κ) obtained from thermal conductance (σ) through their relationship, $\kappa = \sigma L/s$, with cross-sectional area $s = wh$. The thickness $h = 6.033 \text{ \AA}$, and the length $L = 1 \text{ }\mu\text{m}$. σ is calculated by the Landauer formula.